

Monte Carlo simulations of stacked X-ray detectors as designed for SIMBOL-X

Christoph Tenzer^a, Eckhard Kendziorra^a, Andrea Santangelo^a,
Markus Kuster^b, Philippe Ferrando^c, Philippe Laurent^c, Arnaud Claret^d and Rémi Chipaux^d

^aInstitut für Astronomie und Astrophysik, Universität Tübingen,
Sand 1, 72076 Tübingen, Germany

^bInstitut für Kernphysik, TU Darmstadt, Schlossgartenstr. 9, 64289 Darmstadt, Germany

^cUMR 7164 APC & DSM/DAPNIA/Service d'Astrophysique, CEA/Saclay, 91191
Gif-sur-Yvette Cedex, France

^dDSM/DAPNIA/Service d'Astrophysique, CEA/Saclay, 91191 Gif-sur-Yvette Cedex, France

ABSTRACT

SIMBOL-X is a next generation X-ray telescope with spectro-imaging capabilities over the 0.5 to 80 keV energy range. The combination of a formation flying mirror and detector spacecraft allows to extend the focal length to several tens of meters (20 to 30 in the case of SIMBOL-X), resulting in a so far unrivaled angular resolution and sensitivity in the hard X-ray range. The focal plane detector system for SIMBOL-X is planned to consist of an array of so-called Macro Pixel Detectors (MPD) on top of a 2 mm thick CdZnTe pixellated detector array. Photons of energy less than about 17 keV will be primarily absorbed in the MPDs, whereas higher energy photons will be detected in the CdZnTe array below. A computer model of such stacked detectors and its interaction with the radiation environment encountered by the spacecraft in orbit is currently being developed by our group using the Monte Carlo toolkit GEANT4. We present results of the simulation and an outlook for possible optimizations of future detector geometry and shielding.

Keywords: SIMBOL-X, Geant4, stacked detectors, XMM-Newton, pn-CCD, EPIC, background

1. INTRODUCTION TO GEANT4

The GEANT4 toolkit provides a flexible and comprehensive software library package for Monte Carlo simulations that involve the interaction and tracking of particles through matter and electromagnetic fields. It efficiently handles complex particle tracks and geometries and allows their visualization through a variety of interfaces. The implemented physics processes cover electromagnetic interaction of charged hadrons, ions, leptons and photons from 250 eV up to several PeV, hadronic interactions from thermal energies to 1 PeV and also the production and propagation of optical photons. Today the toolkit is freely available at source-code level (object-oriented C++) over the Web¹ and developed and maintained by the GEANT4 Collaboration (see next section).^{2,3}

1.1. Short History of Geant4

The first version of GEANT was written in the FORTRAN programming language in 1974 at CERN* as a framework for tracking only few particles through simple detectors. Since then it has come a long way to the complexity and scale of the current version, the origin of which can be traced back to two independent studies at CERN and KEK[†] in 1993.² Merging these two activities resulted in a project named RD44, a worldwide collaboration involving about one hundred scientists and engineers from Europe, Russia, Japan, Canada and the United States. The first production release of GEANT4 was delivered in 1998 and the number and variety of its applications has been increasing steadily. The GEANT4 Collaboration today considers itself (in terms of size of the code and number of contributors) one of the largest object-oriented and geographically distributed software development projects.²

Further author information: send correspondence to Christoph Tenzer, email: tenzer@astro.uni-tuebingen.de

*Centre Européen pour la Recherche Nucléaire, Geneva, Switzerland

[†]National Laboratory for High Energy Physics, Tsukuba, Japan

The results presented here have been obtained using the current version 4.8.0.p01 of GEANT, which has evolved from previous versions on the basis of the accumulated experience of many contributors to the field of Monte Carlo simulation of detectors and physics processes.

1.2. Design Overview

The key requirements for GEANT4 established by RD44 in the first year of the project were functionality, modularity, extensibility and openness.² This ultimately resulted in a modular and hierarchical structure of the code, which was decided to be developed in an object-oriented approach in the C++ language. It also led to the flexible concept of a 'toolkit', where the user may assemble the simulation from components taken from the toolkit and parts of his own code.

The GEANT4 toolkit today offers the user the possibility to create a geometric model (of a detector or experimental setup) with accurate representation of the physical properties of the involved materials. He may then define sensitive elements that record information needed to simulate a detector response. The user is provided with a whole set of physics processes (see below) - to which he can add his own or modify existing ones - for the behaviour of particles in matter and/or electromagnetic fields from which he can select those relevant for the simulation.

User interaction with the simulation is possible through various interfaces for in-/output parameters, application flow and visualization of the geometries and particle tracks. The simple creation of new interfaces to every aspect of the simulation is a key feature of GEANT4.

1.3. Physics Processes

In GEANT4 a particle is considered *transported* by the simulation rather than being *self moving*. The length of a transportation step (for a particle at rest, this is a time step) is proposed by the physics processes that are associated with the particle at that time. Depending on its nature, a physics process applies to a particle 1) *at rest*, 2) *along step* and/or 3) *post step*.

All physics processes are treated in this same manner from the tracking point of view. GEANT4 provides the user with the following major categories: *electromagnetic*, *hadronic*, *decay*, *photon-hadron* and *optical* processes. For the application described in this paper, i.e. simulating the background of an X-ray detector in a typical space radiation environment, the electromagnetic processes are the most significant of the above mentioned. Descending from the field of high energy physics, GEANT4 distinguishes the so called 'standard' electromagnetic processes from the 'low-energy' electromagnetic processes. The necessary low-energy code data files for photon and electron processes have been included into our simulations in order to increase the accuracy of the simulation down to energies of about 250 eV and to simulate such phenomena as X-ray production through fluorescence.

Long term radioactivity produced by nuclear interactions represents an important contribution to the background levels in space-borne X-ray instruments, as resulting events often occur outside the time-scales of any anticoincidence. To simulate this part of the background, a Radioactive Decay Module that is able to generate the γ - and X-rays associated with electron capture and α -, β^\pm - and isomeric transition decays can be included into the simulations.

2. SIMULATION OF THE XMM-NEWTON PN-CAMERA INTERNAL BACKGROUND

The European Photon Imaging Camera (EPIC) on board of the XMM-Newton satellite consists of three X-ray CCD cameras. Two of them are metal oxide semiconductor (MOS) CCD arrays, while the third uses pn-CCDs and is referred to as the pn-camera.⁴ We chose to simulate the internal background of the pn-camera as a first task to understand and verify the GEANT4 physics processes relevant for an in-orbit X-ray detector. The simulation results can be directly compared to measurements as the background of the pn-camera has been thoroughly investigated and published since the launch of XMM-Newton in December, 1999.⁵

The pn-camera covers an energy range from 0.15 keV to 15 keV with moderate spectral ($E/\Delta E \approx 20-50$) and angular resolution (PSF: 6 arcsec FWHM). It has an imaging area of 6 cm x 6 cm divided into twelve 3 cm x 1

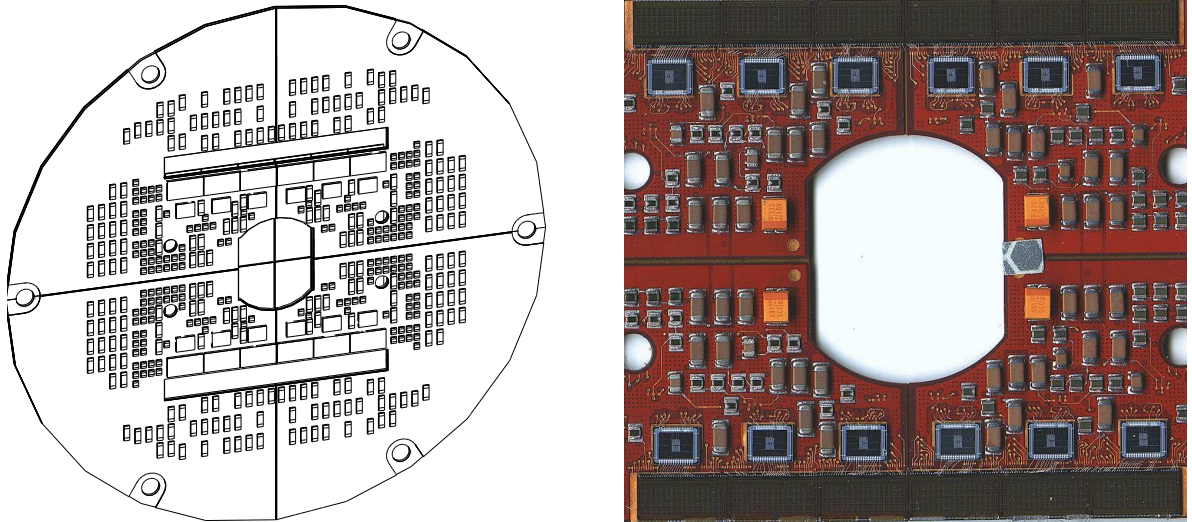


Figure 1. GEANT4 geometrical model (left) of the EPIC-pn focal plane printed circuit board (PCB) and a closeup photo of the area covered (on the backside) by the CCDs on a spare PCB (right). Among the components selected for the simulation are the CAMEX and TIMEX devices for each CCD as well as some smaller SMD components (resistors, capacitors).

cm pn-CCDs on a single wafer with 200×64 pixels each. The pixel size is $150 \times 150 \mu\text{m}^2$ and the covered field of view of the telescope is 30 arcmin.

The measured background can be roughly described as consisting of two parts: the Cosmic X-ray Background (CXB) and the instrumental background. The latter component may be further dissolved into detector noise (below 200-300 eV) and another component which is due to the interaction of high energy particles (above 100 MeV) with the structure surrounding the detector and the detector itself. This component produces a flat photon spectrum inside the detector box that is the dominant source of the background at energies above a few keV. Another contribution to the background that shows a strong and unpredictable variability are so-called *soft proton flares*, which are attributed to low energy protons with energies below ~ 300 keV that are channeled onto the CCDs by the telescope mirrors.

2.1. Simulation

In our simulation we focussed on the X-ray fluorescence triggered by the interactions of the flat photon spectrum mentioned above with the materials inside the detector box close to the CCDs. This phenomenon has been very well measured and has been recently described by Freyberg et al.⁵ For the simulation we created in GEANT4 a model of the CCDs and the focal plane printed circuit board (PCB) underneath the CCDs (see Fig. 1). The PCB consists of a molybdenum core with multiple copper layers on both sides that are divided into quadrants. Through the long rectangular holes, the CAMEX chips are connected via bond wires to the CCDs on the backside of the PCB. The photo on the right of Fig. 1 shows exactly the section that is covered by the CCDs on the other side. When modeling the components of the PCB, we tried to describe their material composition as accurately as possible to produce correct line amplitudes. The CCDs were defined as a sensitive detector for the simulations which measures energy and position of each interaction with particles or photons. The output of these *events* is then stored in FITS-format[‡] conforming to the XMM-Newton eventfile standards and can be further processed to images and spectra with the standard XMM-Newton science analysis software as if it were measured data.

[‡]Flexible Image Transportation System

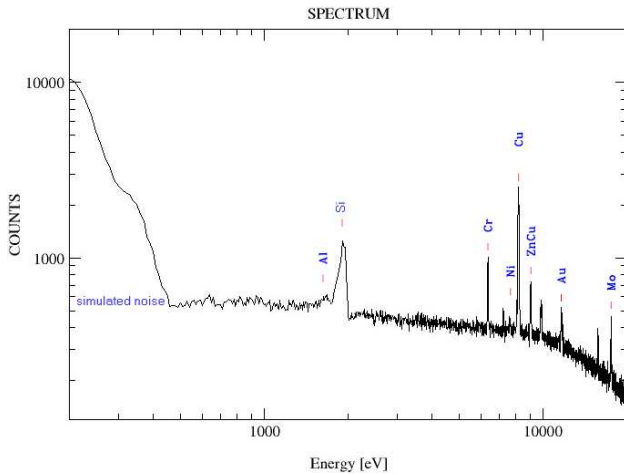


Figure 2. Spectrum generated from the photon events registered by the simulated CCDs showing X-ray fluorescence lines of the materials used for the PCB.

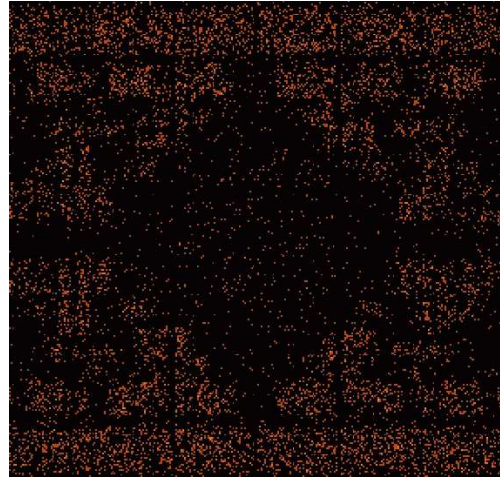


Figure 3. Sample energy slice image, generated of events with energy around the Ni-K α line (7300 - 7600 eV).

2.2. Results

A total of 10^9 isotropically emitted photons following a flat spectrum between 0.1 and 25 keV were created with the GEANT4 General Particle Source (GPS) inside the aluminum camera housing surrounding the PCB. Emphasis was laid on low energy physics processes including X-ray fluorescence emission by the irradiated materials. Time, position and deposited energy of each event inside the CCDs were recorded. The spacial dispersion of the charge cloud produced inside the CCDs by photon interactions was not simulated - thus no split events were produced. The resulting spectrum of this simulation (see Fig. 2) therefore has to be put up against a spectrum with recombined energies when comparing with measured data. Also not considered in this simulation are properties of the CCDs that relate to the readout process (CCE/CTE) or the readout electronics. Simulated Gaussian noise has been added to the spectrum afterwards to account for the electronic detector noise at lower energies. The shape of the fluorescence lines is simulated also with Gaussian distributions, their width corresponding to the respective energy resolution of the pn-camera.

When generating images around the various prominent lines of the spectrum (see Fig. 3), the PCB components where these X-ray fluorescence lines are produced can be identified as containing the respective materials.

2.3. Discussion

The slope of the continuum in Fig. 2 is matching the measured one and the images around the more prominent Cu, Ni and Mo K α -lines can be reproduced fairly well by the simulation. The relative amplitude of some of the lines however is not reproduced correctly. This is most probably due to the fact that not all parts of the camera interior contributing to the fluorescence background have yet been introduced in the geometric model. Soon we will further extend the simulation to include components like e.g. the aluminum shutter directly above the CCDs and the aluminum detector housing and its interaction with high energy particles. The detector housing is also mainly responsible for the strong Al line dominating the measured spectrum. Further simulations will show, how its contribution to the internal background could have been diminished by introducing a graded Z-shield inside the detector.

3. SIMULATIONS CONCERNING SIMBOL-X

SIMBOL-X is an X-ray mission that uses a ~ 20 m focal length mirror to focus X-rays with energies between 0.5 and 80 keV. The focal length will be achieved by a formation flying configuration of a mirror spacecraft and a

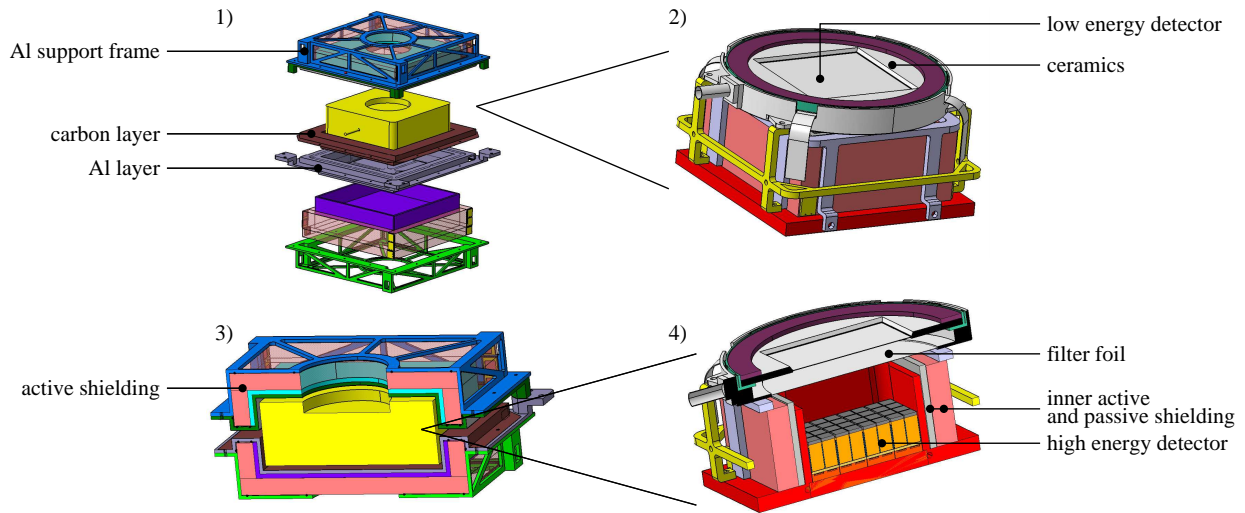


Figure 4. Baseline mechanical model of the SIMBOL-X focal plane. 1) Detector box - exploded view, 2) mechanical model of the inner detector assembly, 3) cut through the detector box, 4) cut through the inner detector assembly (B.P.F. Dirks et al.⁹).

detector spacecraft. After the end of a Phase 0 assessment study in autumn 2005, SIMBOL-X has been selected by CNES[§] for a one year Phase A study.

The SIMBOL-X telescope on the mirror spacecraft will be made of about one hundred Wolter Type-I nested shells, for the fabrication of which the industrial partners have already acquired a large experience through the building of the BeppoSAX, SWIFT and XMM-Newton mirrors. To ward off radiation from angles adjacent to the observing direction, the mirror spacecraft holds a 3 m diameter sky baffle.

The detector spacecraft is carrying the detector box with the high- and low-energy detectors and a collimator. The low-energy detector (LED) will be a MACRO PIXEL detector (developed by the Semiconductor Laboratory (HLL) of the Max-Planck-Institut für extraterrestrische Physik (MPE) and Werner-Heisenberg-Institut (WHI)), which is an array of depleted Field Effect Transistors (DEPFETs), each of them surrounded by a silicon drift chamber to increase the sensitive area. Prototypes of MACROPIXEL detectors have already been developed, built and tested by the HLL.⁶⁻⁸ The LED consists of 128 x 128 pixels with a baseline size of 500 x 500 μm^2 with 450 μm depletion depth and will be operated in a nominal energy range of 0.5 keV to 20 keV. The detector is logically and functionally divided into four quadrants of 64 x 64 pixels each that will be read out in parallel at a frame time of 256 μs . This short integration time allows the operation of the detector even at room temperature. In order to reduce thermal noise and to achieve an energy resolution of <145 eV (FWHM) at 5.9 keV, the wafer must be cooled down to only -30°C.⁹

The high-energy detector (HED) of SIMBOL-X is a mosaic constructed of 8 x 8 Cd(Zn)Te crystals (10 x 10 x 2 mm³) covered with 256 pixels of about 500 x 500 μm^2 . Each crystal has its own readout electronics (developed by CEA/Saclay) located directly in a cube below. The HED will operate in the energy range of 5 to 100 keV, partially overlapping the LED's energy range. To fulfill the scientific objectives depicted below, a high energy resolution of about 1 keV at 60 keV is required. Prototypes of pixellated Cd_{0.9}Zn_{0.1}Te detectors are currently under study in Saclay.⁹

Taking the above described baseline parameters into account, the SIMBOL-X mission will provide unprecedented sensitivity and angular resolution with respect to non-focusing telescopes and will cover the sensitivity gap between XMM-Newton and the INTEGRAL observatory. To reach the intended sensitivity of below 1 μCrab ,

[§]Centre National d'Études Spatiales, French space agency

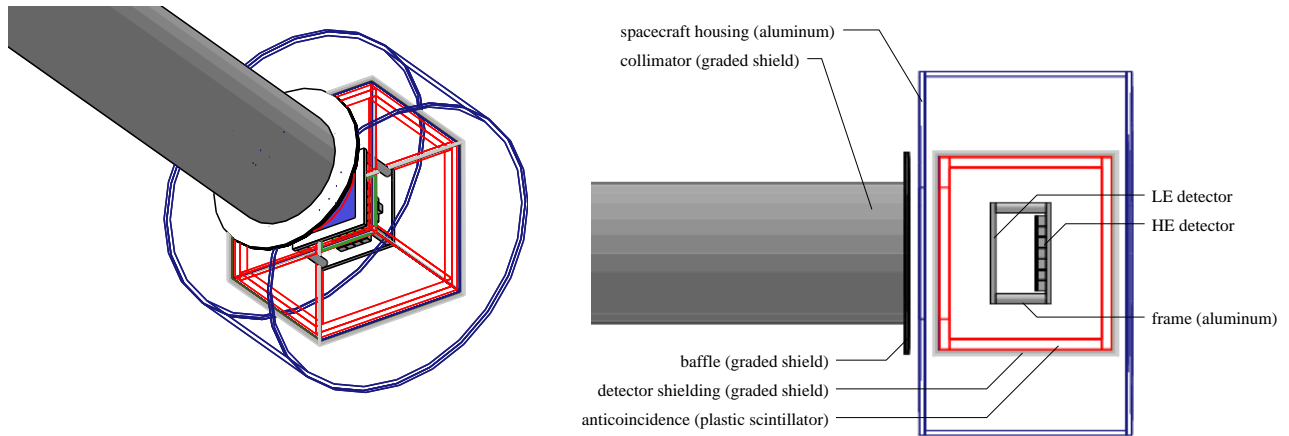


Figure 5. Preliminary geometric model used for the GEANT4 simulations of the SIMBOL-X detector. Wireframe 3D-view on the left and longitudinal section on the right.

the detectors need to show a very low residual background, the simulation of which is the present work of our group.

SIMBOL-X is now undergoing a phase A study, leading to a flight decision in the second quarter of 2007, with the launch scheduled 2013. The satellites will be placed in a highly excentric orbit of seven days (perigee: 44,000 km, apogee: 253,000 km) to minimize the radiation level, resulting in six days of scientific observation and one day for data downlink and formation correction. Scientific objectives include the dynamics of matter around compact objects, acceleration processes in supernova remnants, the controversial presence of a non-thermal X-ray component in clusters of galaxies and the Cosmic X-ray Background.^{10,11}

3.1. Geometric Model of the Detector Spacecraft

A detailed mechanical model of the current baseline configuration of the detector housing and the detectors is shown in Fig. 4. The central elements of the geometric model are the two detectors that are interconnected through an aluminum frame. They are surrounded by an anti-coincidence shield (AC), which will most likely be consisting of plastic scintillator slabs that are connected to photo diodes. A graded shield is foreseen around or inside the AC to reduce the incoming photon flux. Its current baseline configuration is (from outside to inside) *tantalum* (1.3 mm), *tin* (2.2 mm), *copper* (0.48 mm), *aluminum* (0.27 mm) and *carbon* (0.1 mm) with a total thickness of 4.35 mm, leaving X-ray fluorescence below 0.3 keV and therefore below the detection limit of the LED. Different materials and geometric configurations for the active and passive shielding are under consideration at the moment. An aluminum structure encloses and stabilizes the active parts of the camera.

Above the aperture of the detector box, there is a 1.4 m long collimator to prevent photons coming from directions other than the FOV from hitting the detectors. It is also made of the materials that make up the graded shield. Its thickness, however, is decreasing with the distance from the detector to save weight and to maintain a constant effective thickness with respect to the incident angle of the incoming radiation. The model of the spacecraft used in our simulations is a simplified version of the mechanical model. A 3D-view and a longitudinal cut through the detector spacecraft are shown in Fig. 5.

3.2. Simulation of the Performance of the Collimator

Regarding the geometrical setup of the detector spacecraft, we first focussed on the performance of the collimator. Therefore 10^8 photons with an energy following the CXB spectrum (as compiled by D. E. Gruber et al.¹²) were fired at the detector spacecraft from the solid angle covered by the collimator. The countrates in both detectors were then recorded for different thickness settings of the collimator materials. Our aim was to show by simulation which thickness would suffice to reduce the background below the desired 10^{-4} counts/s/cm²/keV.

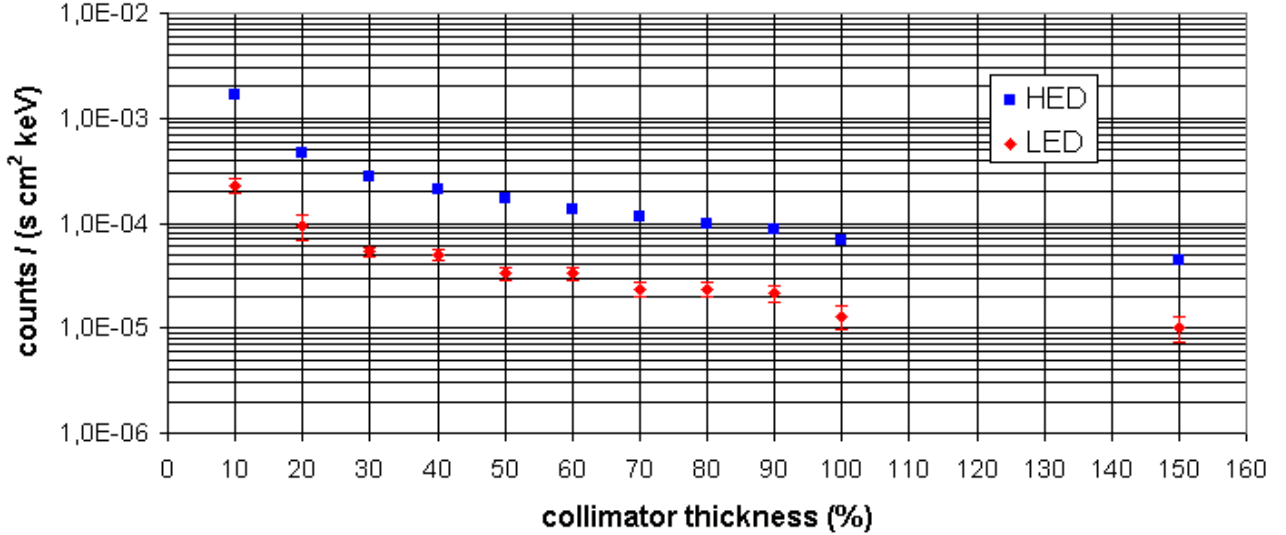


Figure 6. Simulated countrates in the high and low energy detector as a function of collimator thickness (100% corresponds to 4.35 mm of graded shield, see also Sect. 3.1; HED errors are smaller than plot symbols).

From the number of simulated photons and the input spectrum a virtual ‘exposure time’ can be calculated. In order to do this, the input spectrum has to be integrated over the energy range of the LED, the solid angle covered by the collimator and the active area of the LED. This value is then compared to the number of LED counts without collimator, taking into account the LED’s quantum efficiency. Combining this exposure time with the number of hits on each detector, the detector area and the energy bandwidth, a background countrate for each detector as a function of the collimator thickness can be specified. The results of the simulations are shown in Fig. 6. An exponential decrease in the countrates with increasing thickness of the collimator is clearly observable and the thickness where the background drops below the above mentioned value is $\sim 30\%$ for the LED and $\sim 90\%$ of the standard settings for the graded shield for the HED.

When restricting the input spectrum (CXB) to energies below 100 keV (which is the value for up to which the collimator thickness was originally optimized by using a simple analytical model targeted at the center of the field of view), the LED detects no more photons at a collimator thickness $> 25\%$ and at 100% no more photons are registered on both detectors. Regarding the parameters used in the simulations this can be expressed as countrates of less than 7.1×10^{-7} counts/s/cm²/keV for the LED and less than 1.5×10^{-7} counts/s/cm²/keV for the HED. The resulting background spectrum shows for 100% thickness no fluorescence lines from the collimator.

3.3. Simulation of the Proton-Induced Background

Another simulation study has been performed, with the purpose to estimate the level of prompt background induced by the cosmic proton flux and to quantify the efficiency of the anticoincidence shield for the rejection of this background. In that study, a slightly different geometry was used but with the same basic shielding components. Protons were shot isotropically at the whole spacecraft, in a range of energy between 10 MeV and 100 GeV. The simulations give directly the number of interactions in LED and HED and the deposited energy. Figure 7, for example, gives the number of interactions in the energy-range of interest (supposed to be 1 to 100 keV in HED and 0.5 to 15 keV in LED). Convolution with the cosmic proton flux calculated for a solar active year with the code CREME86¹³ gives the counting rates reported in Table 1.

4. OUTLOOK

To test the properties of the AC and the effectiveness of the shielding for the detector box itself, a test bench has been developed where different materials for the AC (CsI, BGO, plastic) and various configurations for the

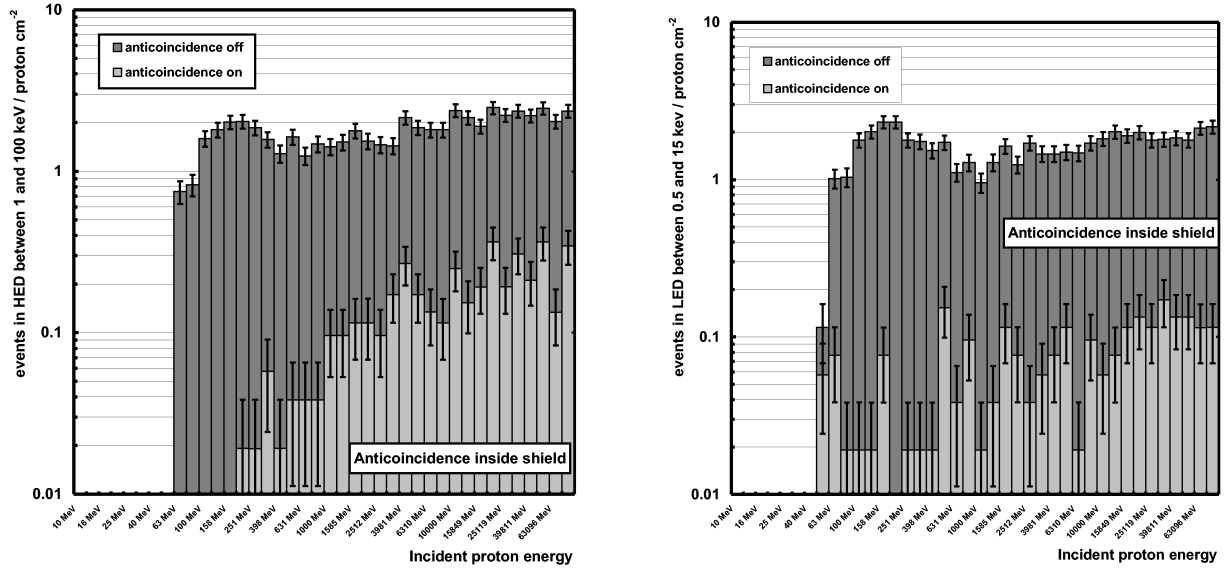


Figure 7. Mean number of interactions in the range of energy per proton $\cdot \text{cm}^{-2}$ in HED (right) and LED (left). Anticoincidence is inside the passive graded shield.

Table 1. Calculated mean count rates in LED and HED due to cosmic protons, without (anticoincidence off) and after (anticoincidence on) veto. Rates in detectors are given for per cm^2 and per keV. Statistical errors on the last digits are indicated in parenthesis.

	Anticoincidence inside shield	Anticoincidence outside shield
Anticoincidence off		
Countrates in LED:		
Total ($E_{LED} > 0$)	1.383(3) counts/s/cm ² /keV	1.377(4) counts/s/cm ² /keV
In range ($0.5 < E_{LED} < 5$ keV)	$8.39(22) \times 10^{-3}$ counts/s/cm ² /keV	$6.27(27) \times 10^{-3}$ counts/s/cm ² /keV
Over range ($E_{LED} > 15$ keV)	1.375(3) counts/s/cm ² /keV	1.370(4) counts/s/cm ² /keV
Countrates in HED:		
Total ($E_{HED} > 0$)	$217.9(4) \times 10^{-3}$ counts/s/cm ² /keV	$215.1(6) \times 10^{-3}$ counts/s/cm ² /keV
In range ($1 < E_{HED} < 100$ keV)	$1.03(3) \times 10^{-3}$ counts/s/cm ² /keV	$0.69(3) \times 10^{-3}$ counts/s/cm ² /keV
Over range ($E_{HED} > 100$ keV)	$216.9(4) \times 10^{-3}$ counts/s/cm ² /keV	$2.144(6) \times 10^{-3}$ counts/s/cm ² /keV
Anticoincidence on		
Countrates in LED:		
Total ($E_{LED} > 0$)	$6.46(17) \times 10^{-3}$ counts/s/cm ² /keV	$11.5(3) \times 10^{-3}$ counts/s/cm ² /keV
In range ($0.5 < E_{LED} < 5$ keV)	$0.37(5) \times 10^{-3}$ counts/s/cm ² /keV	$0.20(4) \times 10^{-3}$ counts/s/cm ² /keV
Over range ($E_{LED} > 15$ keV)	$6.09(16) \times 10^{-3}$ counts/s/cm ² /keV	$11.3(3) \times 10^{-3}$ counts/s/cm ² /keV
Countrates in HED:		
Total ($E_{HED} > 0$)	$2.66(4) \times 10^{-3}$ counts/s/cm ² /keV	$1.13(4) \times 10^{-3}$ counts/s/cm ² /keV
In range ($1 < E_{HED} < 100$ keV)	$0.07(1) \times 10^{-3}$ counts/s/cm ² /keV	$0.02(1) \times 10^{-3}$ counts/s/cm ² /keV
Over range ($E_{HED} > 100$ keV)	$2.59(4) \times 10^{-3}$ counts/s/cm ² /keV	$1.11(3) \times 10^{-3}$ counts/s/cm ² /keV

graded shield can be simulated in a typical space radiation environment. The experience from this test bench will contribute to the decisions of whether to put the AC slabs inside or outside the shielding, whether a thin foil is required between the two detectors for additional shielding (and what material it should be made of) as well as to the overall geometric setup of the detector box. Adding an active shield to the base of the collimator is also an option that is considered and already queued for simulation. This could further reduce the background in the HED.

The part of the background that is due to delayed emission from material that became activated by protons will also be investigated by our group.

ACKNOWLEDGMENTS

This work was partly supported by Bundesministerium für Wirtschaft und Technologie through Deutsches Zentrum für Luft- und Raumfahrt e.V. (DLR) grants FKZ 50QR0503 and FKZ 50OX002.

REFERENCES

1. S. Giani et al., “An object-oriented toolkit for simulation in HEP,” <http://geant4.web.cern.ch>, *CERN/LHCC* **98-44**, July 1998.
2. S. Agostinelli et al., “Geant4 - a simulation toolkit,” *Nuclear Instruments and Methods in Physics Research A* **506**, pp. 250–303, July 2003.
3. J. Allison et al., “Geant4 developments and applications,” *IEEE Transactions on Nuclear Science* **53**, pp. 270–278, 2006.
4. L. Strüder et al., “The European Photon Imaging Camera on XMM-Newton: The pn-CCD camera,” *A&A* **365**, pp. L18–L26, Jan. 2001.
5. M. J. Freyberg, U. G. Briel, K. Dennerl, F. Haberl, G. D. Hartner, E. Pfeffermann, E. Kendziorra, M. G. F. Kirsch, and D. H. Lumb, “EPIC pn-CCD detector aboard XMM-Newton: status of the background calibration,” in *X-Ray and Gamma-Ray Instrumentation for Astronomy XIII. Edited by Flanagan, Kathryn A.; Siegmund, Oswald H. W. Proceedings of the SPIE, Volume 5165, pp. 112-122 (2004).*, K. A. Flanagan and O. H. W. Siegmund, eds., pp. 112–122, Feb. 2004.
6. J. Treis et al., “Noise and spectroscopic performance of DEPMOSFET matrix devices of XEUS,” in *Proceedings of the SPIE*, **5898**, pp. 256–266, 2005.
7. J. Treis et al., “Advancements in DEPMOSFET device developments for XEUS,” in *Proceedings of the SPIE*, **6276-17**, 2006.
8. L. Strüder et al., “Active X-ray pixel sensors with scalable pixel sizes from $1\mu\text{m}^2$ to $10^8\mu\text{m}^2$ in Heaven and on Earth,” in *Proceedings of the SPIE*, **6276-48**, 2006.
9. B.P.F. Dirks et al., “The focal plane of the SIMBOL-X space mission,” in *Proceedings of the SPIE*, **6276-45**, 2006.
10. P. Ferrando et al., “SIMBOL-X: a formation flying mission for hard-x-ray astrophysics,” in *Optics for EUV, X-Ray, and Gamma-Ray Astronomy II. Edited by Citterio, Oberto; O’Dell, Stephen L. Proceedings of the SPIE, Volume 5900, pp. 195-204 (2005).*, pp. 195–204, Aug. 2005.
11. P. Ferrando et al., “SIMBOL-X: mission overview,” in *Proceedings of the SPIE*, **6266-17**, 2006.
12. D. E. Gruber, J. L. Matteson, L. E. Peterson, and G. V. Jung, “The Spectrum of Diffuse Cosmic Hard X-Rays Measured with HEAO 1,” *The Astrophysical Journal* **520**, pp. 124–129, July 1999.
13. A. Claret, “Space environment of SIMBOL-X,” in *DAPNIA/SAp/CRS internal note*, Feb. 2006.